Neuroscience Research 93 (2015) 144–157

Contents lists available at ScienceDirect

Neuroscience Research

journal homepage: www.elsevier.com/locate/neures

Comparative analyses of adeno-associated viral vector serotypes 1, 2, 5, 8 and 9 in marmoset, mouse and macaque cerebral cortex

Akiya Watakabe[a,b,*], Masanari Ohtsuka[a], Masaharu Kinoshita[c,1], Masafumi Takaji[a], Kaoru Isa[c], Hiroaki Mizukami[d], Keiya Ozawa[d,2], Tadashi Isa[b,c], Tetsuo Yamamori[a,b]

[a] Division of Brain Biology, National Institute for Basic Biology, Okazaki, Japan
[b] Graduate University for Advanced Studies (SOKENDAI), Okazaki, Japan
[c] Department of Developmental Physiology, National Institute for Physiological Sciences, Okazaki, Japan
[d] Division of Genetic Therapeutics, Center for Molecular Medicine, Jichi Medical University, Japan

ARTICLE INFO

Article history:
Received 1 August 2014
Received in revised form 26 August 2014
Accepted 27 August 2014
Available online 18 September 2014

Keywords:
rAAV
Tropism
Viral vector
Monkey
Non-human primate
Neuron

ABSTRACT

Here we investigated the transduction characteristics of adeno-associated viral vector (AAV) serotypes 1, 2, 5, 8 and 9 in the marmoset cerebral cortex. Using three constructs that each has hrGFP under ubiquitous (CMV), or neuron-specific (CaMKII and Synapsin I (SynI)) promoters, we investigated (1) the extent of viral spread, (2) cell type tropism, and (3) neuronal transduction efficiency of each serotype. AAV2 was clearly distinct from other serotypes in small spreading and neuronal tropism. We did not observe significant differences in viral spread among other serotypes. Regarding the cell tropism, AAV1, 5, 8 and 9 exhibited mostly glial expression for CMV construct. However, when the CaMKII construct was tested, cortical neurons were efficiently transduced (>∼70% in layer 3) by all serotypes, suggesting that glial expression obscured neuronal expression for CMV construct. For both SynI and CaMKII constructs, we observed generally high-level expression in large pyramidal cells especially in layer 5, as well as in parvalbumin-positive interneurons. The expression from the CaMKII construct was more uniformly observed in excitatory cells compared with SynI construct. Injection of the same viral preparations in mouse and macaque cortex resulted in essentially the same result with some species-specific differences.

1. Introduction

Adeno-associated viral vectors (AAVs) have now become one of the standard tools for gene delivery into central nervous system. Transduction of neurons with optogenetic molecules, for example, provides unprecedented opportunities to manipulate neural circuit (Betley and Sternson, 2011; Fenno et al., 2011; Han, 2012). To produce recombinant AAV particles, the transcription unit of interest is sandwiched between the two inverted terminal repeat sequences (ITRs) of AAV, which is packaged with capsids provided in trans. One characteristic feature of AAV is that there exist a huge number of different serotypes that exhibit unique species- and tissue tropism (Rabinowitz et al., 2002; Klein et al., 2008; Wu et al., 2006). The capsids derived from these serotypes can be used to package the transfer vector of AAV2 to confer unique transduction properties and cell tropisms (Rabinowitz et al., 2002).

To date, many studies have investigated the transduction properties of AAV serotypes for the nervous system. AAV1, 2, 5, 8 and 9 have been shown to transduce neurons and glias in the striatum, hippocampus, neocortex, substantia nigra, retina and amygdala among others (Burger et al., 2004; Cearley and Wolfe, 2006; Taymans et al., 2007; Klein et al., 2008; Blits et al., 2010; Hutson et al., 2012; Aschauer et al., 2013; Holehonnur et al., 2014). Other serotypes such as AAV6, AAV7, AAV-DJ, AAVRh10, and AAVRh43 are potentially useful but less well examined (Aschauer et al., 2013; Cearley and Wolfe, 2006; Holehonnur et al., 2014; Klein et al., 2008). Most of these studies were done for rodents, but some studies focused on non-human primates (Dodiya et al., 2010; Markakis et al., 2010; Masamizu et al., 2011; Sanchez et al., 2011). What became clear from these analyses is that the extent of viral spread and the cell tropism could be quite different between serotypes depending on the target tissue and species. Therefore, it

* Corresponding author at: 38 Nishigonaka, Myodaijicho, Okazaki, Aichi 444-8585, Japan. Tel.: +81 564 55 7616; fax: +81 564 55 7617.
E-mail address: watakabe@nibb.ac.jp (A. Watakabe).
[1] Present address: Department of Physiology, Hirosaki University School of Medicine, Hirosaki, Japan.
[2] Present address: IMSUT Hospital, The Institute of Medical Science, The University of Tokyo, 4-6-1 Shirokanedai, Minato-ku, Tokyo 108-8639, Japan.

http://dx.doi.org/10.1016/j.neures.2014.09.002

is desirable to use the appropriate AAV serotypes for transduction according to the needs of each experiment.

This study started from the motivation to identify the appropriate serotypes to transduce cortical neurons of the non-human primates, in particular, marmosets. Marmoset, a small New World Monkey, is a good model organism for neuroscience research (Clarke et al., 2004; Bendor and Wang, 2005; Okano et al., 2012) and we are interested in using it as a model to investigate the primate-specific architecture of the cerebral cortex (Yamamori and Rockland, 2006; Watakabe et al., 2012). To begin with, we injected various AAV serotypes containing a GFP reporter under ubiquitous CMV promoter to marmoset cortex. Unexpectedly, we observed mainly glial expression for AAV1, 5, 8 and 9, which appeared to contradict past studies (Nathanson et al., 2009; Blits et al., 2010; Masamizu et al., 2010). This led us to investigate the transduction efficiency of AAV serotypes using neuron-specific promoters such as CaMKII and SynI promoters. For comparison, we also injected the same preparation of AAVs to mouse and macaque cortex. We describe and discuss the transduction properties of five AAV serotypes that emerged from a series of our analyses.

2. Materials and methods

2.1. Ethics statement

All the experiments were conducted in accordance with the guideline of the National Institutes of Health, and the Ministry of Education, Culture, Sports, Science and Technology (MEXT) of Japan, and were approved by the Institutional Animal Care and Use Committee of National Institutes of Natural Sciences. We made all efforts to minimize the number of animals used and their suffering.

2.2. Plasmid construction

The constructs used in this study are schematically shown in Fig. 1O. The CMV-hrGFP construct (pAAV-hrGFP) was obtained from Agilent Technologies Inc. (originally obtained from Stratagene). The CMV promoter and beta-globin intron sequences were excised and replaced either with SynI promoter (Hioki et al., 2009) and CaMKII promoter (CaMKII alpha 1.3: a gift from Drs. Ryosuke Matsui and Dai Watanabe, Kyoto University) to make SynI and CaMKII constructs.

2.3. Viral injection

Adeno-associated viral (AAV) vectors used in this paper have ITRs of AAV2 and with capsids of serotype 1, 2, 5, 8 and 9. They were produced in HEK 293 cells by using a helper virus free system and purified by two times CsCl2 density gradients and titrated by Q-PCR as described previously (Yagi et al., 2011). Our vector titration results were consistent with those quantified in reference to the international standard, which was recently used in a multicenter collaborative study (Lock et al., 2010). Final preparations were dialyzed against PBS and adjusted to 0.5×10^{13} GC (genome copies)/ml for CMV construct and 0.4×10^{13} GC/ml for CaMKII and SynI constructs.

Seven adult marmosets (*Callithrix jacchus*) of both sexes were used in this study (Table 1). Following an intramuscular injection of ketamine/xylazine mixture (30 mg/kg, 1.3 mg/kg, respectively), deep anesthesia was induced by isoflurane (1–2%) inhalation. The head of the marmoset was fixed to the stereotaxic apparatus and surgery was carried out under continuous monitoring of the heart rate and the rectal temperature. A small hole was made in the skull using a dental drill. The viral vector was delivered by pressure injection using a glass micropipette attached either to a nanoliter 2000 injector connected to Micro4 controller (World Precision instrument), or to a microinfusion pump (Harvard Apparatus). To inject virus into the brain, the dura was punctured using a tip of 27G needle, through which the glass pipette was slowly lowered to the target depth. Approximately 0.5, 0.63 or 0.63 μl (for CMV, CaMKII or SynI constructs, respectively) of the viral solutions containing 2.5×10^9 GC were injected at the rate of 0.1 or 0.125 μl/min. The pipette was held in place for 2 min before and after the injection. After retracting the glass micropipette, the hole was filled with Spongel, an absorbable gelatin sponge (Astellas Pharma Inc.) and the head skin was sutured. The marmosets were sacrificed three or six weeks after injection.

Table 1
Marmosets used in this study.

ID	Construct	Serotypes	Expression
#1	CMV-hrGFP	AAV1, 2	3 weeks
#2	CMV-hrGFP	AAV5, 8, 9	3 weeks
#3	CMV-hrGFP	AAV1, 9	6 weeks
#4	CaMKII-hrGFP	AAV1, 2, 8, 9	6 weeks
	SynI-hrGFP	AAV1, 2, 8, 9	
#5	CaMKII-hrGFP	AAV1, 2, 5, 8, 9	6 weeks
#6	CaMKII-hrGFP	AAV5, 9	3 weeks
#7	CMV-hrGFP	AAV1	3 weeks
	CaMKII-hrGFP	AAV1	

Fourteen adult C57BL6J mice of either sex (17–28 weeks) were anesthetized with an intraperitoneal injection of ketamine/xylazine mixture (100 mg/kg, 10 mg/kg, respectively). The virus injection was performed in a similar manner as described above for marmoset. In these mice, approximately 0.5 μl of the viral solutions injected into somatosensory area (AP + 1 mm, left 3 mm, depth 0.5 mm). These mice were sacrificed three weeks after injection.

Eight hemispheres of four adult macaque monkeys (two male *Macaca mulatta*, male and female *Macaca fuscata*) were used. Under the same surgical procedure reported previously (Kinoshita et al., 2012), the injections were made after the craniotomy at the frontal lobe and the occipital lobe. After incision of the dura or making a small hole on the dura with 18-gauge needle, the glass micropipette (tip diameter 100–120 μm) was penetrated at the depth 0.4 mm and/or 0.8–1.0 mm from the cortical surface of the occipital lobe, at 1.0–1.5 mm for frontal lobe or at 3.0 mm in the frontal lobe near the central sulcus. Approximately 0.5 or 0.8 μl of the viral solutions, which had the same constructs and titer as those used in the marmosets, were injected into each site at the rate of 0.1 μl/min under the control of a microinfusion pump (Eicom). The pipette was held in place for 5 min after the injection. After the retraction of the micropipette, the dura was sutured (if necessary) and covered with Spongel (Astellas Pharma Inc.), and the skin was sutured. The animals were sacrificed six-eight weeks after the injections.

2.4. Immunostaining and data analyses

Animals were anesthetized with sodium pentobarbital and perfused transcardially with 0.9% NaCl, followed by fixation with 4% paraformaldehyde in 0.1 M phosphate buffer, pH 7.4. The fluorescent signals of hrGFP were strong enough to be detected without enhancement by immunodetection. For some experiments, however, we performed antibody staining using anti-hrGFP to clearly distinguish the fluorescent signals from the background autofluorescence. For immunofluorescence, the sections were treated with 80% methanol/20% dimethyl sulfoxide solution (Dent's solution) for more than 30 min. After washing, the sections were blocked with 10% fetal bovine serum, 2% bovine serum albumin, and 0.5% Triton X-100 in TBS, pH 7.4, followed by overnight incubation

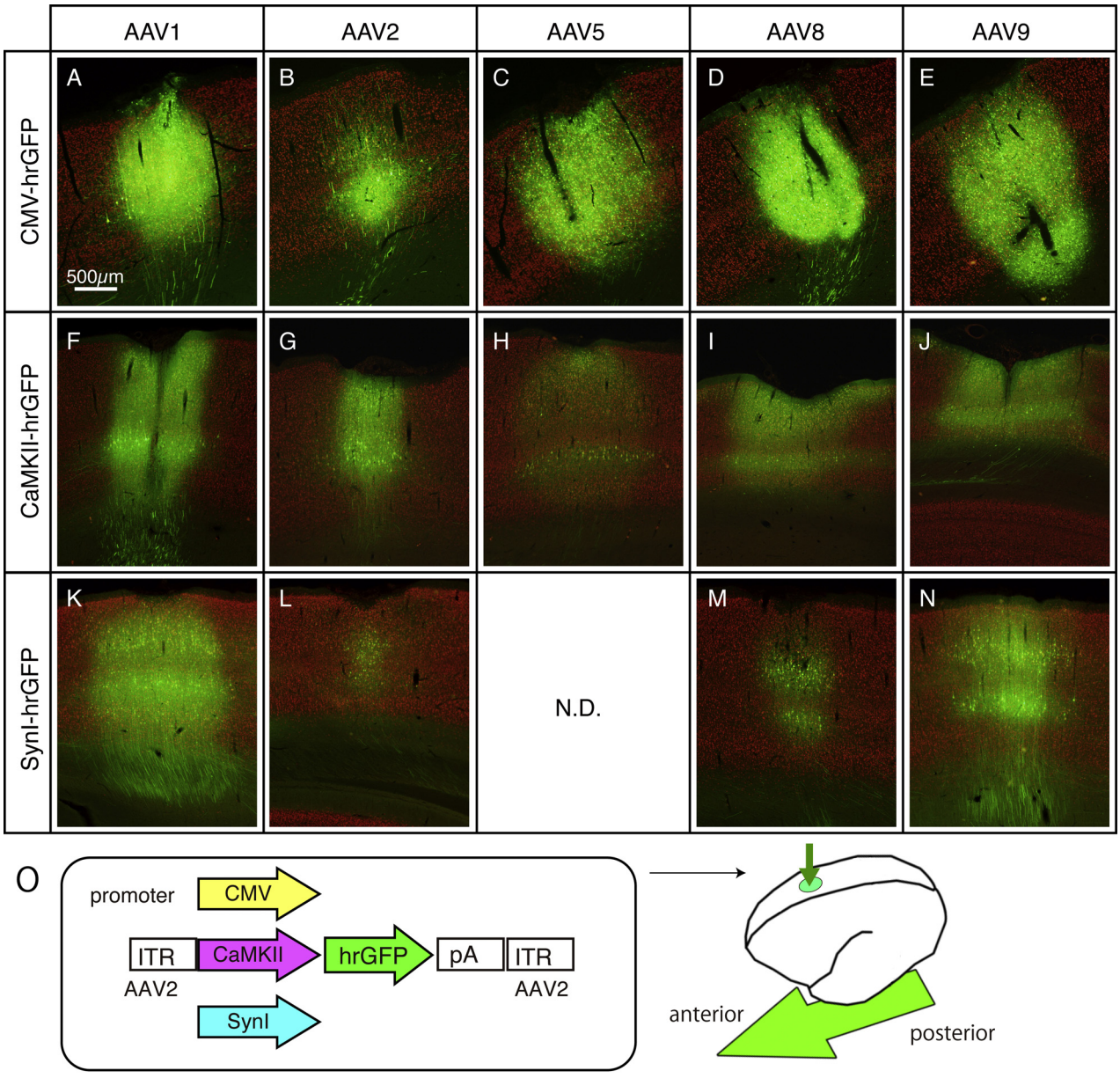

Fig. 1. Various AAVs injected into marmoset cerebral cortex. AAV constructs containing CMV, CaMKII, and SynI promoters driving hrGFP expression were packaged in AAV1, 2, 5, 8, and 9 capsids and injected into the marmoset cerebral cortex. The low-magnified images of representative sections are shown for each combination. These are merged views for hrGFP (green) and NeuN (red) signals. To aid visualization, the contrasts of images are adjusted. So that we can directly compare the signal intensities across serotypes, the sections for the same promoters were immunostained simultaneously, imaged and contrast-adjusted in exactly the same conditions. These images were taken from marmosets ID#1 and #2 for CMV promoter (panels A–E), ID#5 for CaMKII promoter (panels F–J) and ID#4 for SynI promoter (panels K–N). Panel O shows the schematic views of the AAV constructs and injections. The arrow indicates the anterior–posterior axis. (For interpretation of the references to color in this figure legend, the reader is referred to the web version of this article.)

with the primary antibody for hrGFP (rabbit polyclonal, 1:4000; Agilent Technology #240141), and for NeuN (mouse monoclonal, Millipore, MAb377) at 4 °C. After incubation with fluorophore-conjugated secondary antibodies, the sections were counterstained with Hoechst 33342 (1:2000; Molecular Probes). The fluorescent images were captured by Olympus DP71 digital camera attached to BX51 microscope (Olympus). The confocal images were taken by Nikon confocal laser microscope system A1. Maximum intensity projection images for the confocal data were created by NIS-Elements imaging software (Nikon). All the images were processed by Adobe Photoshop for proper contrast for presentation.

For measurement of viral spread, a circle was drawn to cover the center of the transduction and the radius was measured. Viral spread in layers 2 and 5 was ignored, because it unpredictably goes beyond the circle. In counting the neuronal transduction efficiency of CaMKII-construct, a single optical section of hrGFP/NeuN/Hoechst stained section was captured using 40× objective lens. A ROI with 150 μm × 150 μm size was selected from the image. We first identified NeuN positive cell bodies. To avoid the interference of strong fluorescence that is not directly on the optical section, we counted only the NeuN-positive cells with clear nuclear signals as positive. As to the hrGFP signals, most of the imaged field was filled with green signals after adjusting the contrast, and it was often difficult to distinguish the cell bodies from the surrounding tissue only by the green fluorescence. In such cases, we counted the cells as positive, because the transgene-negative cells can be differentiated by lack of fluorescence.

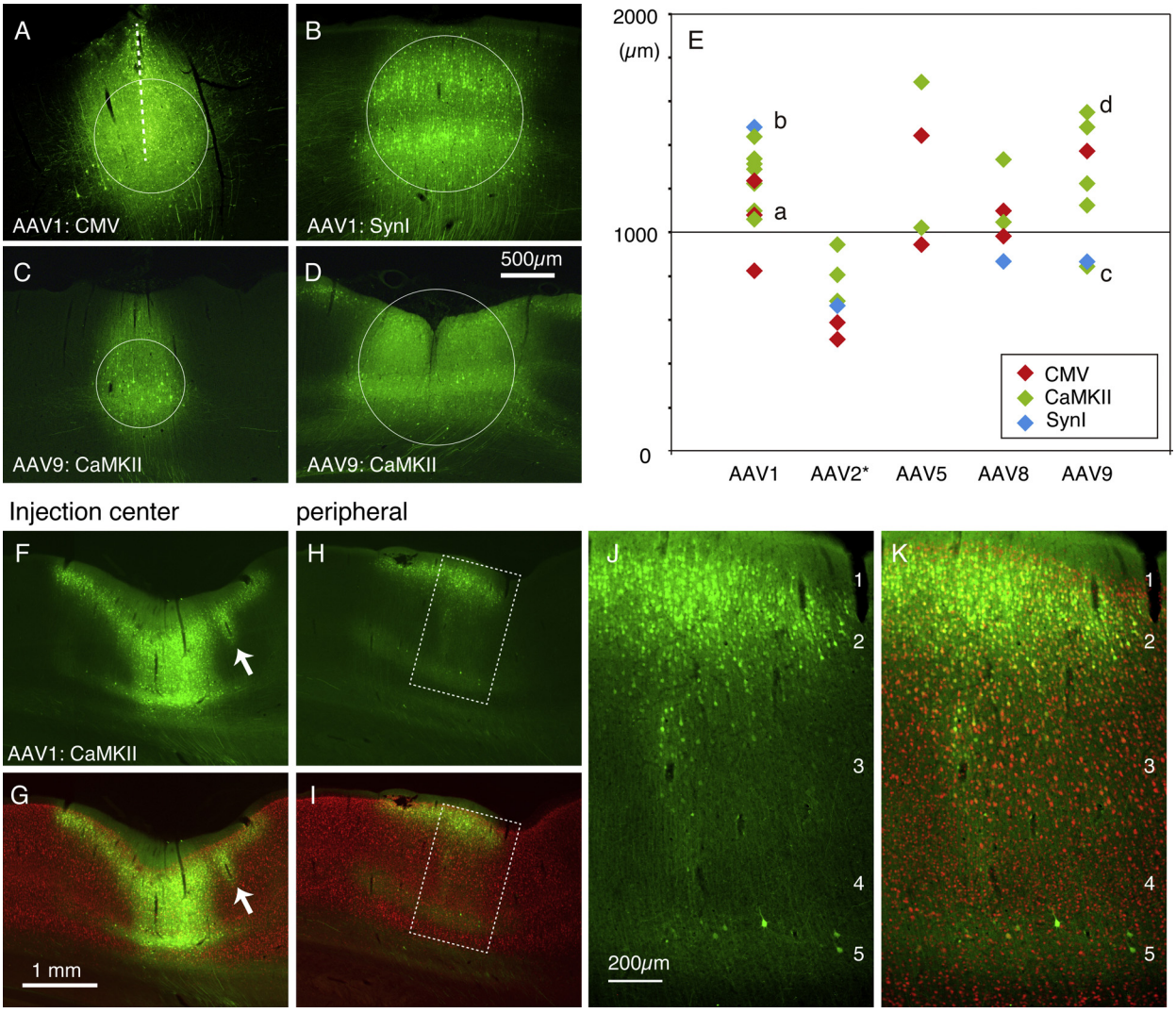

Fig. 2. Estimation of viral spread for various serotypes. (A–D) The extent of viral spread was measured using a circle. In determining this circle, we ignored the widespread distributions in layers 2 and 5 and set the radius to cover layer 3 expression. The examples of measurement shown in panels A–D indicate that the infection occurred along the cortical column and not along the needle track (white dotted line in panel A). The magnification is the same for panels A–D. (E) The red, green and blue plots represent the radius of viral spread for CMV, CaMKII and SynI promoters, respectively. Each plot represents independent injections. The plots indicated by a–d represent the values for the white circles shown in panels A–D. *When the results of different promoters were mixed, the statistically significant difference was observed only for AAV2 being smaller than other cell types ($p < 0.001$ between AAV1/5/9 and AAV2 and $p < 0.05$ between AAV8 and AAV2, Ryan's method). (F and G) An example of viral spread in layers 2 and 5 beyond spherical diffusion. Panel F shows hrGFP signals of AAV1/CaMKII-hrGFP injection, while panel G shows a merge with NeuN (red). The arrow indicates viral infection along the blood vessel. (H and I) The hrGFP and hrGFP-NeuN merged views of a section peripheral to the injection center. This section was approximately 1 mm lateral from the section shown in panels F and G. The white dotted boxes are magnified in panels J and K. The magnification is the same for panels F–I. (J and K) The hrGFP and hrGFP-NeuN merged views of the white dotted squares in panels H and I. Note high and dense expression in layer 2 as well as sparse expression in layer 5. (For interpretation of the references to color in this figure legend, the reader is referred to the web version of this article.)

3. Results

3.1. Marmoset cortical neurons are efficiently transduced by AAV serotypes 1, 2, 5, 8 and 9

The specific aim of the current study is to clarify how various AAV serotypes transduce the neurons of the cerebral cortex of marmosets, mice and macaques. We used three different promoters to drive hrGFP expression, namely, CMV, CaMKII and SynI promoter (Fig. 1O). CMV promoter is ubiquitous, but in the context of AAV construct, the cell-type tropism depends on the serotypes of the capsid (Aschauer et al., 2013). CaMKII and SynI promoters are both neuron-specific. A previous study suggested preferential expression in excitatory and inhibitory neurons for these promoters, respectively, when packaged in AAV1 capsids (Nathanson et al., 2009).

Fig. 1 shows the hrGFP expression from these three constructs packaged in AAV1, 2, 5, 8 and 9 in the marmoset cortex. As this figure shows, all the AAV vectors we tested exhibited efficient transduction of cortical cells. At this low magnification, the differential property of each injection was manifested in three aspects. First, there existed considerable differences in the extent of viral spread. On first look, the transduced area of AAV2 was smaller than other serotypes. Second, the overall signal intensities were variable. This was most conspicuous for AAV5/CaMKII-hrGFP: although viral spread was as efficient as AAV8 and 9 (Fig. 1I and J), the expression level per cell was much lower for AAV5 (Fig. 1H). Finally, the distribution of hrGFP signals was not uniform and exhibited characteristic patterns for each promoter. For example, we observed intense cell body signals that span all layers for CMV promoter (Fig. 1A–E), while more diffuse uniform labeling with weak layer 4 was observed for CaMKII promoter (Fig. 1F–J). On the other hand,

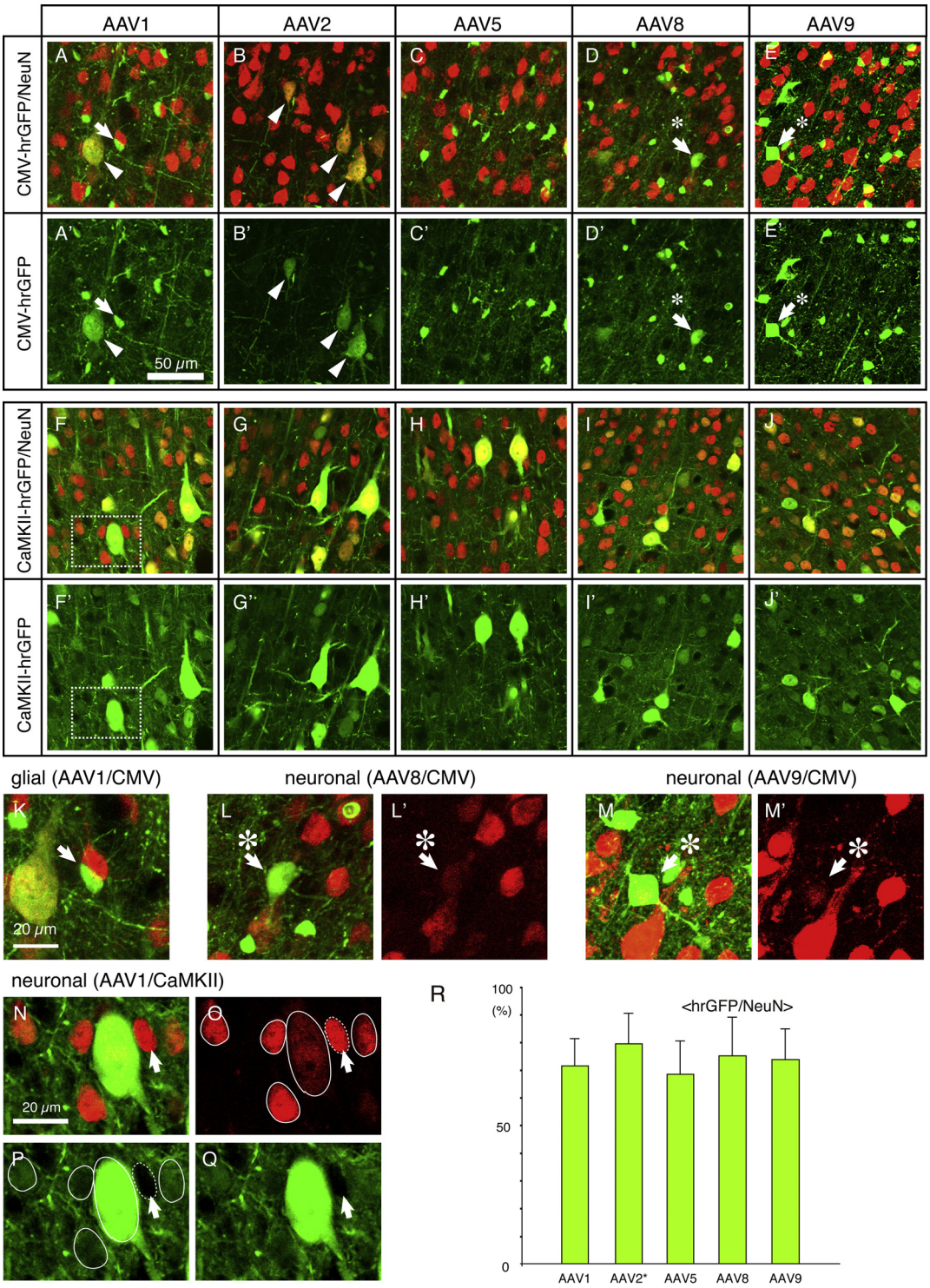

Fig. 3. Glial and neuronal expression of transgene from AAV serotypes. Marmoset cortical sections were immunostained with anti-hrGFP (green) and anti-NeuN antibody (red) to differentiate neuronal and glial transduction. A single optical section of confocal microscopy images are shown in each panel. These images were taken from layer 5. (A–E) Merged views for hrGFP (green) and NeuN (red) signals of AAV1, 2, 5, 8 and 9 coding CMV-hrGFP. (A′–E′) Only hrGFP signals are shown for the same images as A–E. The arrowheads indicate neurons. The arrows indicate hrGFP-positive cells with apparently no NeuN signals. Among these, the arrows with stars were actually considered to be neurons (see panels K–M). (F–J) Merged views for hrGFP (green) and NeuN (red) signals of AAV1, 2, 5, 8 and 9 coding CaMKII-hrGFP. The dotted rectangle in panels F and F′ are magnified in panels N–Q. (K) The cells shown by the arrow in panel A was magnified. This is a typical example of a glia apposed to a neuron. (L and L′) The cell shown by the arrow with a star in panels D and D′ was magnified. This cell has a neuronal morphology and weak NeuN signal. (M and M′) The cell shown by the arrow with a star in panels E and E′ was magnified. This cell also has a neuronal morphology and weak NeuN signal. (N–O) Magnified views of dotted rectangle in panels F and F′. There is only one cell that is obviously positive for hrGFP. Among other cells that are positive for NeuN, the one indicated by the arrow clearly lacks hrGFP signal (see panel Q) and is considered to be negative for hrGFP (shown by dotted circle in panels O and P). We consider other three NeuN positive cells to be also positive for hrGFP (shown by circle). (R) The ratio of hrGFP-positive cells among the NeuN-positive cells in layer 3 (average: bar standard deviation; $n = 7$ for AAV1, $n = 4$ for AAV2 and 5, $n = 6$ for AAV8 and $n = 10$ for AAV9). See materials and methods for more detail. (For interpretation of the references to color in this figure legend, the reader is referred to the web version of this article.)

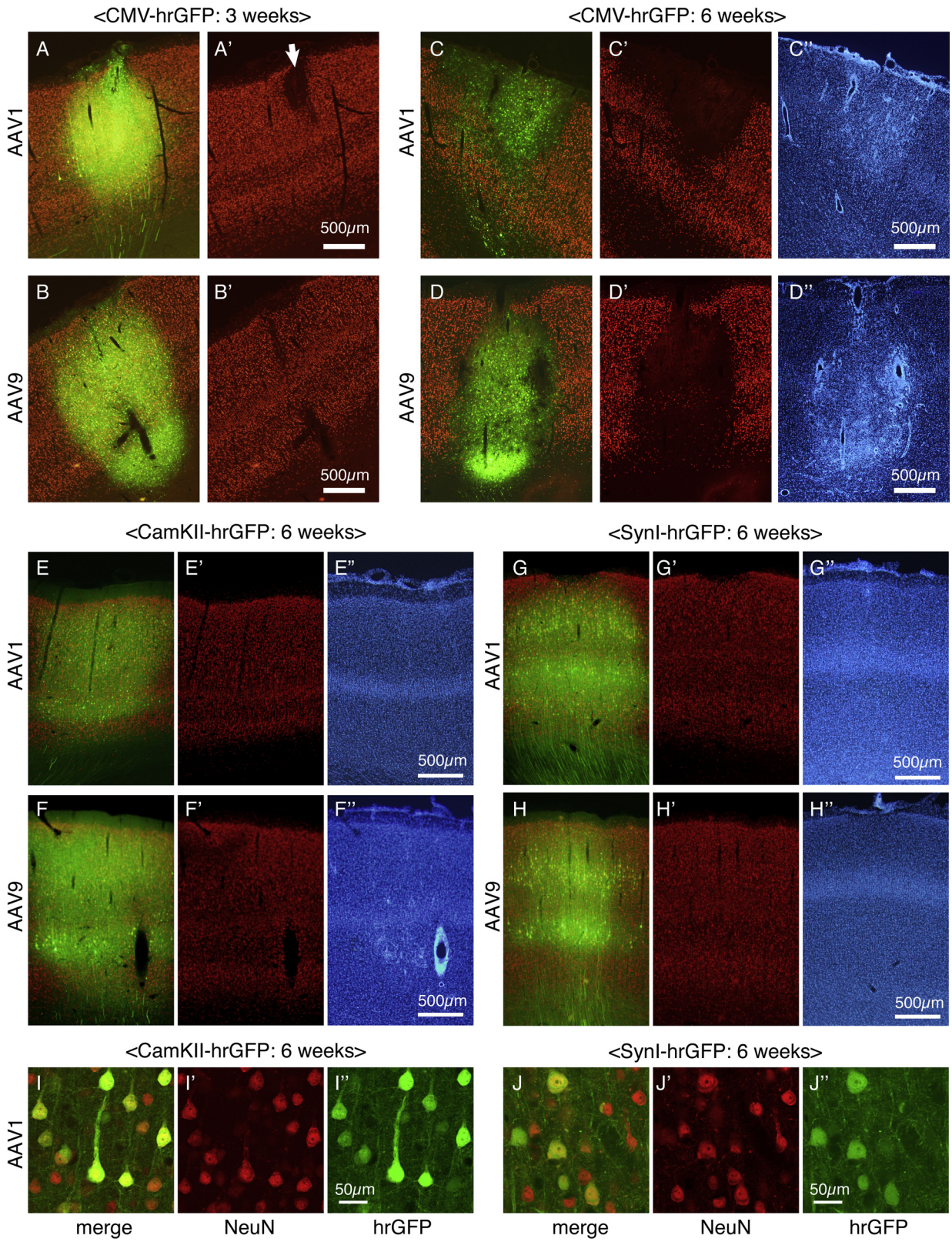

Fig. 4. Toxicity of AAV transduction for CMV-promoter construct. The toxicity of AAV transduction was monitored by reduction of NeuN signals and infiltration of glia cells. (A and B) AAV1 or AAV9/CMV-hrGFP construct was injected into the marmoset cortex and examined for transgene expression (green) after 3 weeks (marmoset #1 and 2). At this magnification, we did not observe substantial changes in the level of NeuN (red), although at higher magnification, the strong hrGFP-positive cells tended to show lower level of NeuN (e.g., Fig. 3L and M). (C and D) AAV1 or AAV9/CMV-hrGFP construct was injected into the marmoset cortex and examined for transgene expression after 6 weeks (marmoset #3). In this example, we observed residual expression of hrGFP in the glia cells with loss of NeuN-positive neurons (see panels C′ and D′). In panels C″ and D″, the infiltration of glia cells were observed by strong and dense nuclear staining by Hoechst33342. (E and F) AAV1 or AAV9/CaMKII-hrGFP construct was injected into the marmoset cortex and examined for transgene expression after 6 weeks (marmoset #4). Some glial infiltration was observed for AAV9 (see panel F″). (G and H) AAV1 or AAV9/SynI-hrGFP construct was injected into the marmoset cortex and examined for transgene expression after 6 weeks (marmoset #4). (I) A magnified view of AAV1/CaMKII-hrGFP construct showing no effect of hrGFP expression (green) on the level of NeuN (red). (J) A magnified view of AAV1/SynI-hrGFP construct. (For interpretation of the references to color in this figure legend, the reader is referred to the web version of this article.)

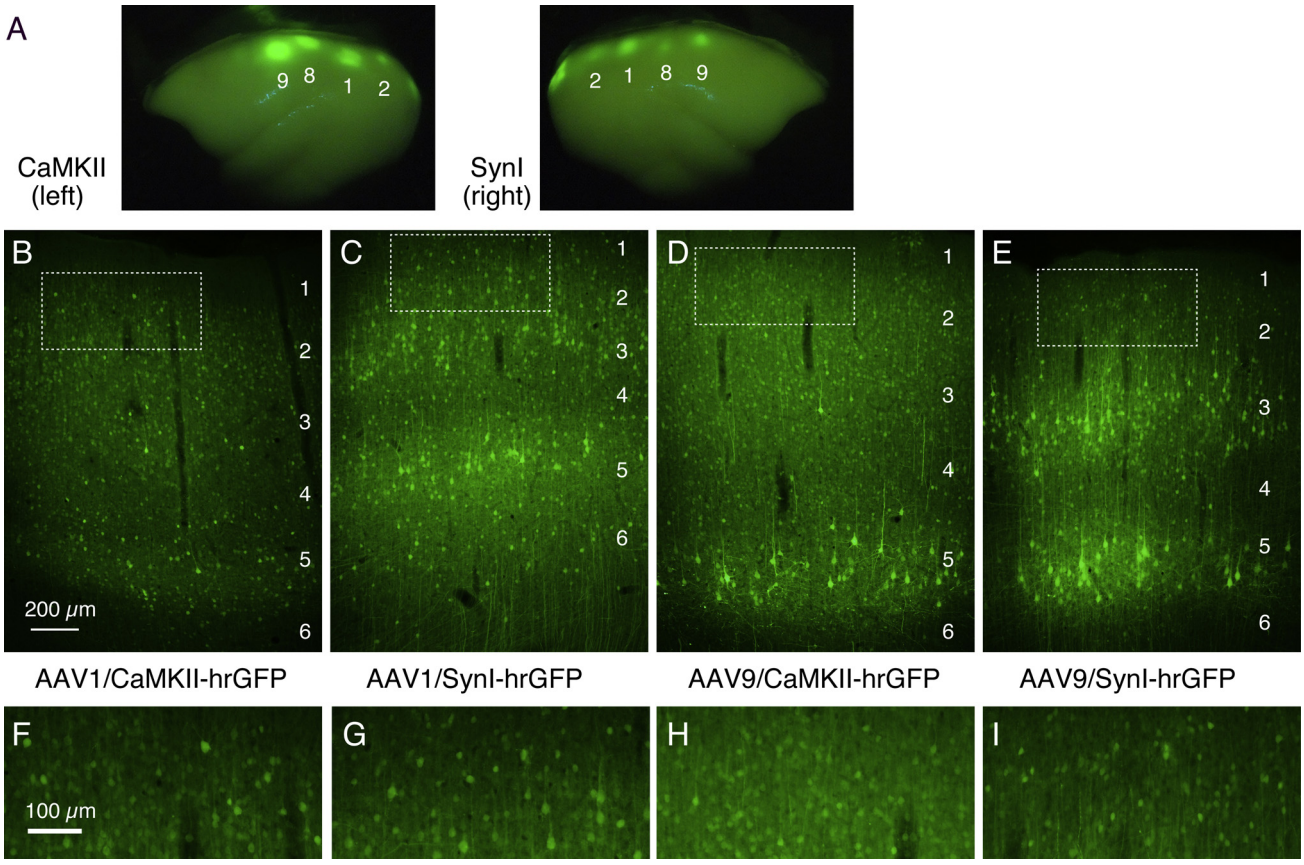

Fig. 5. Comparison of CaMKII and SynI construct. (A) An overview of a marmoset brain (#4) that received AAV/CaMKII-hrGFP on the left hemisphere and AAV/SynI-hrGFP on the right hemisphere. The number indicates the serotypes injected. (B–E) Comparison of unstained sections for CaMKII and SynI constructs in AAV1 and 9 capsids. These fluorescent images were taken in the same conditions using a 10× objective, using fluorescent microscope. (F–I) The dotted boxes in panels B–E were magnified. Note that weakly stained cells are more numerous in CaMKII construct than SynI construct.

SynI promoter showed weak diffuse staining with strong cell body signals in layers 3 and 5 (Fig. 1K–N). Such patterns are considered to arise as a combined result of differential cell tropism of each serotype and the cell type specificity of the promoter activity.

With this picture in mind, we analyzed the differential behavior of AAV serotypes in (1) extent of viral spread, and (2) cell type specificity and transduction efficiency of each AAV vector in more detail. In addition, we describe our data on the cell toxicity and cell type specificity of CaMKII promoter in comparison with CMV and SynI promoter. We also compared our data on marmoset cortex with the results in mouse and macaque monkeys to aid comparison of past studies.

3.2. *Spreading profiles of various AAV serotypes in the marmoset cerebral cortex*

The spread of AAV particles for different serotypes were estimated on the assumption that the viral spread is affected by the capsids but not by promoters. Since the diffusion of the viral particles from the injection point is expected to be spherical, we used a circle to determine the extent of viral spread (Fig. 2A–D). In practice, we observed two patterns of non-spherical transduction. In most cases, the transduction occurred in a columnar fashion beyond the limit of spherical diffusion. Such spread likely reflects the columnar architecture of the cortex and not caused by spread along the needle track, because the infection in some cases occurred oblique to the needle track (white dotted line in Fig. 2A). Secondly, we sometimes encountered very widespread transduction to occur in layers 2 and 5. Fig. 2D and F–I show typical cases of widespread transduction. The layer 2 transduction in such cases can spread as far as several millimeters. This is seen in transverse section in Fig. 2F and G, as well as in layer2/5 specific distribution of hrGFP-positive cells in the peripheral sections (Fig. 2H–K). As shown in magnified views, the infection in layer 2 was quite dense even in the peripheral region, whereas infection in layer 5 mainly occurred sparsely in large pyramidal cells (Fig. 2J and K). This type of spread is qualitatively distinct from the columnar spread and was ignored in determining the circle. We set the radius to cover layer 3 expression (see Fig. 2A–D as examples). We also ignored a sporadic infection that seems to have occurred along the blood vessel (see the arrow in Fig. 2F).

Fig. 2E shows the summary of all the injection data. ANOVA showed that the distribution of AAV2 is statistically different from other serotypes ($p < 0.001$). AAV1, 5 and 9 spread as wide as 1.2 ± 0.2, 1.3 ± 0.3, 1.2 ± 0.4 mm (means ± SD), respectively, whereas the distribution of AAV2 was 0.7 ± 0.2 mm. We could not observe statistical differences between AAV1, 5, 8 and 9.

3.3. *Efficiency of neuronal transduction by AAV serotypes*

We next examined the cell type preference and transduction efficiency of various AAV serotypes by counterstaining with NeuN antibody for neuronal identification. Confocal microscopic observation at high magnification revealed that the densities of hrGFP-positive cells were unexpectedly very low for CMV-hrGFP construct, compared with those of NeuN positive neurons (Fig. 3A–E). For AAV2, the obviously strong signals were sparse but they were mostly observed in neurons (Fig. 3B). For other serotypes, most of the strongly positive cells for AAV1, 5, 8 and 9 totally lacked

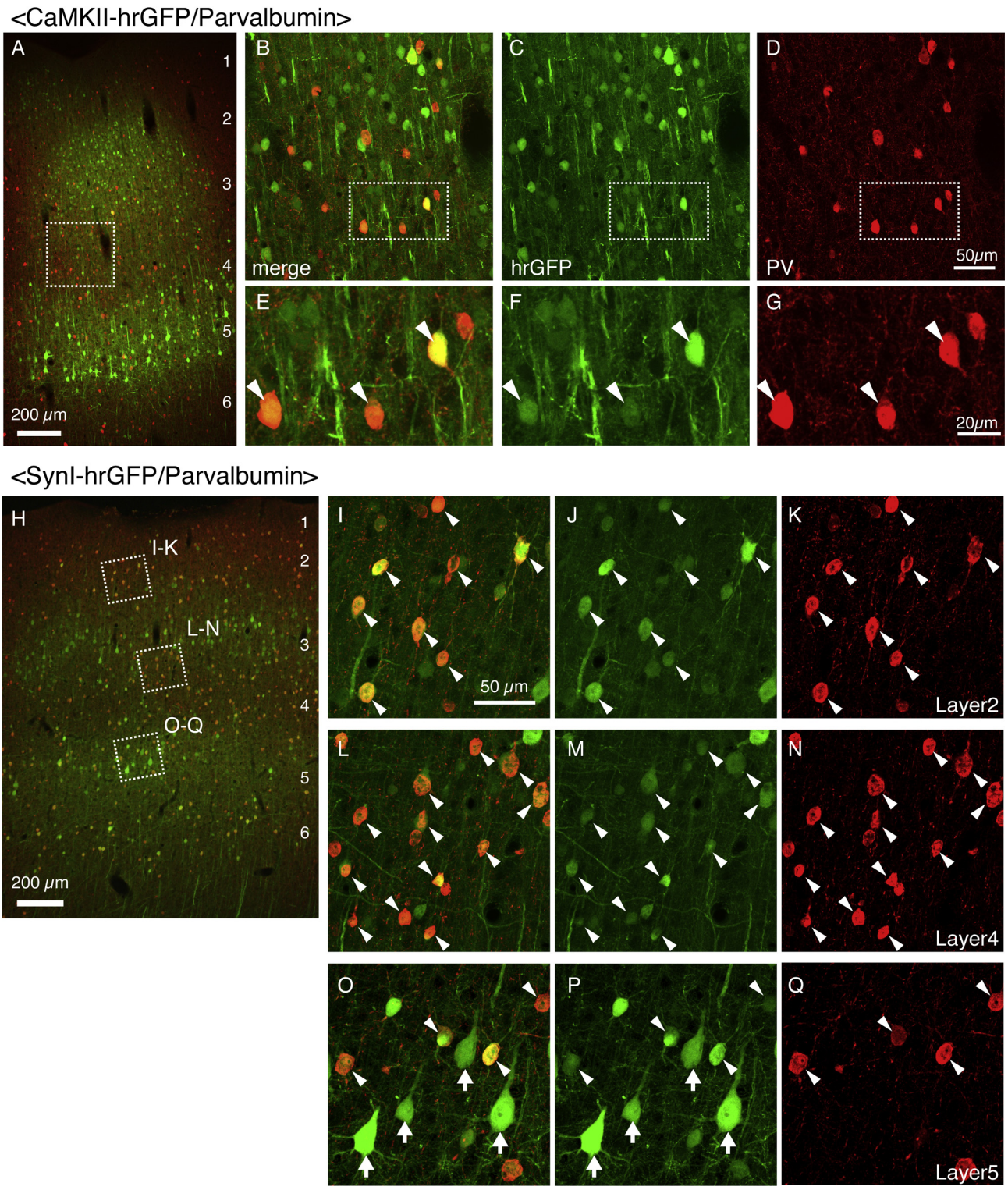

Fig. 6. GABAergic expression of hrGFP driven by CaMKII and SynI promoters. (A) An AAV1/CaMKII-hrGFP injected sample was immunostained with PV antibody (red). (B–D) High power views of the dotted rectangle in panel A. (E–G) High power views of dotted rectangles in panels B–D, respectively. The arrowheads indicate hrGFP-positive PV cells. (H) An AAV1/SynI-hrGFP injected sample was immunostained with PV antibody (red). (I–Q) High power views of the dotted rectangles in layers 2 (I–K), 4 (L–N) and 5 (O–Q) of panel A. The arrowheads indicate hrGFP-positive PV cells. Note high coincidence of hrGFP (green) and PV (red) signals. In layer 5 (O–Q), large pyramidal cells (indicated by arrows) were strongly positive for hrGFP and negative for PV. (For interpretation of the references to color in this figure legend, the reader is referred to the web version of this article.)

NeuN signals and exhibited size and morphology characteristic of glial cells (e.g., Fig. 3K). For AAV1, we observed some strong positive signals to be colocalized with NeuN signals (Fig. 1A, arrowhead). For AAV5, 8 and 9, there were very few NeuN-positive cells with hrGFP expression. However, we observed relatively large hrGFP-positive cells to exhibit very low level of NeuN signals, which are likely to be neuronal cells with repressed NeuN signals (Fig. 2L and M; see below for more analyses on cell toxicity). The “granular”

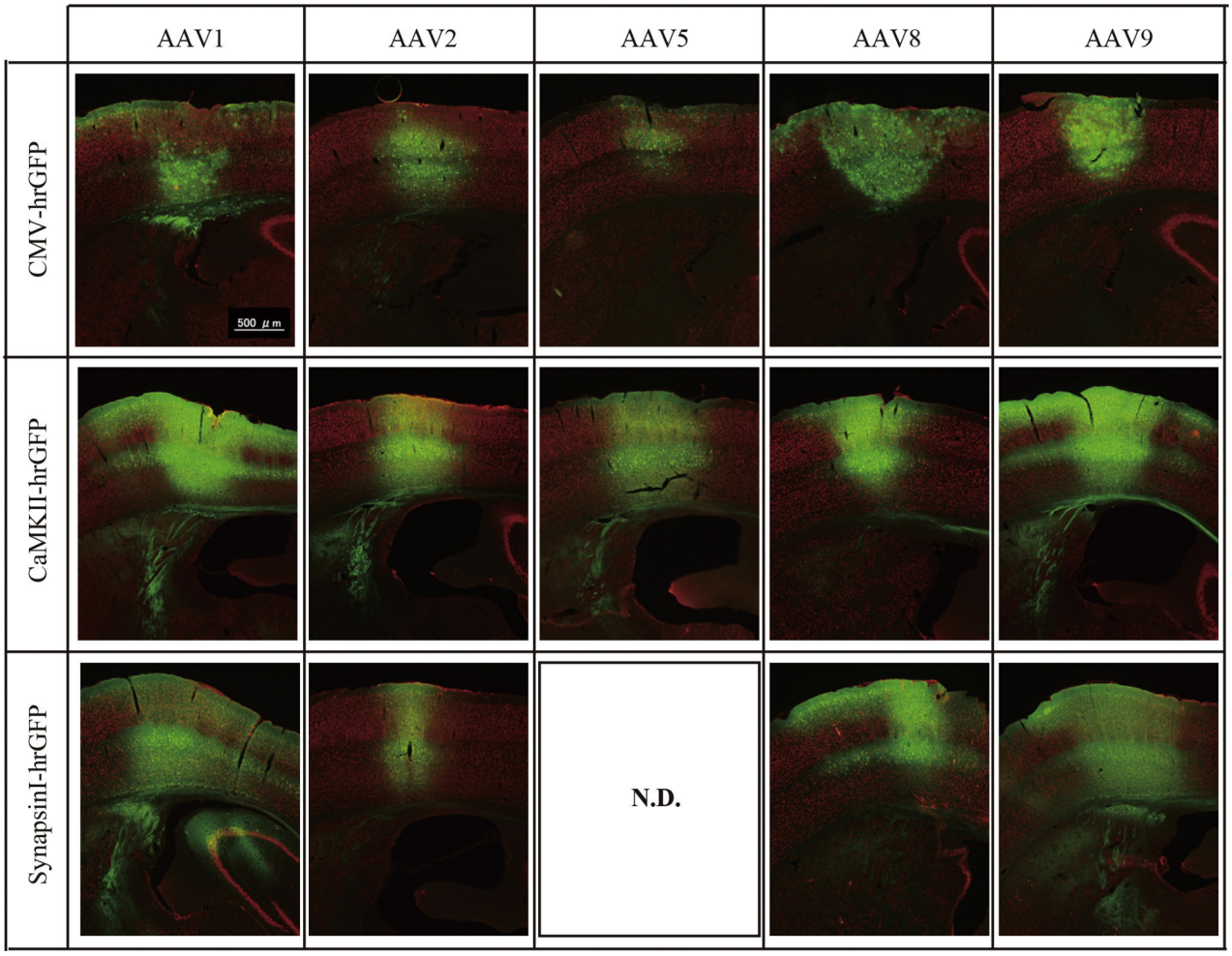

Fig. 7. AAV serotypes injected into mouse barrel cortex. AAV constructs containing CMV, CaMKII, and SynI promoters driving hrGFP expression were packaged in AAV1, 2, 5, 8, and 9 capsids and injected into the mouse barrel cortex. The low-magnified images of representative sections are shown for each combination. These are merged views for hrGFP (green) and NeuN (red) signals. To aid visualization, the contrasts of images are adjusted. So that we can directly compare the signal intensities across serotypes, the sections for the same promoters were immunostained simultaneously, imaged and contrast-adjusted in exactly the same conditions. (For interpretation of the references to color in this figure legend, the reader is referred to the web version of this article.)

appearance of CMV construct at low magnification is, therefore, explained by the sparseness of strongly positive cells, which are mostly neuronal for AAV2 and glial for other serotypes.

We next examined the transduction profiles of CaMKII-hrGFP construct. As expected, almost all of the hrGFP-positive cells were neurons, as judged by colocalization with NeuN signals (Fig. 3F–J). On the other hand, the ratio of hrGFP-positive cells among the NeuN positive cells appeared to be low for all the serotypes at first glance: some NeuN-positive cells expressed hrGFP at high level and others at moderate level, but the majority of the NeuN-positive cells were "as green as" the surrounding extracellular space (e.g., surrounded by circles in Fig. 3O and P). Although such images give the impression that most neurons are negative for hrGFP, we considered these cells to be hrGFP-positive for the following reasons. First, these images are single optical sections of confocal microscopy. It is highly likely that the hrGFP signals are contained within the NeuN stained cell bodies. Second, there exist hrGFP negative spots that are clearly darker than the surrounding tissues. These spots are considered to be the true hrGFP-negative cells (e.g., Fig. 3N–Q, arrow). There are also hrGFP-negative spots with no NeuN staining. These spots are probably glias, because they have Hoechst-stained nuclear (data not shown). Third, the texture of the staining suggests that there exist a cell body surrounded by extracellular space. With this criteria (see methods for detail), over ~70% of the neurons in layer 3 were transduced by AAV/CaMKII-hrGFP in the core region of infection, regardless of serotypes (Fig. 3R). This result was supported by double in situ hybridization with hrGFP and VGluT1 probes (data not shown). We consider that the "extracellular space" actually consists of matrices made of neuropils of transduced neurons.

To conclude, as far as the CaMKII promoter is used, the neuronal transduction efficiency is not very different between the serotypes. At the titer we used, the majority of the neurons in the core of injection were transduced, and a subpopulation of neurons expressed the transgene at very high level.

3.4. Cell toxicity caused by CMV-promoter driven hrGFP expression

We showed in Fig. 3L and M that some neurons with high hrGFP expression exhibited low level of NeuN signals. This observation raised the possibility that high hrGFP expression may repress NeuN expression and have general toxic effect on neurons. This was especially true for AAV5, 8 and 9, for which almost no NeuN-positive cells exhibited strong hrGFP signals (Fig. 3D and E). The data shown for CMV promoter in Fig. 3 was obtained from a marmoset that had

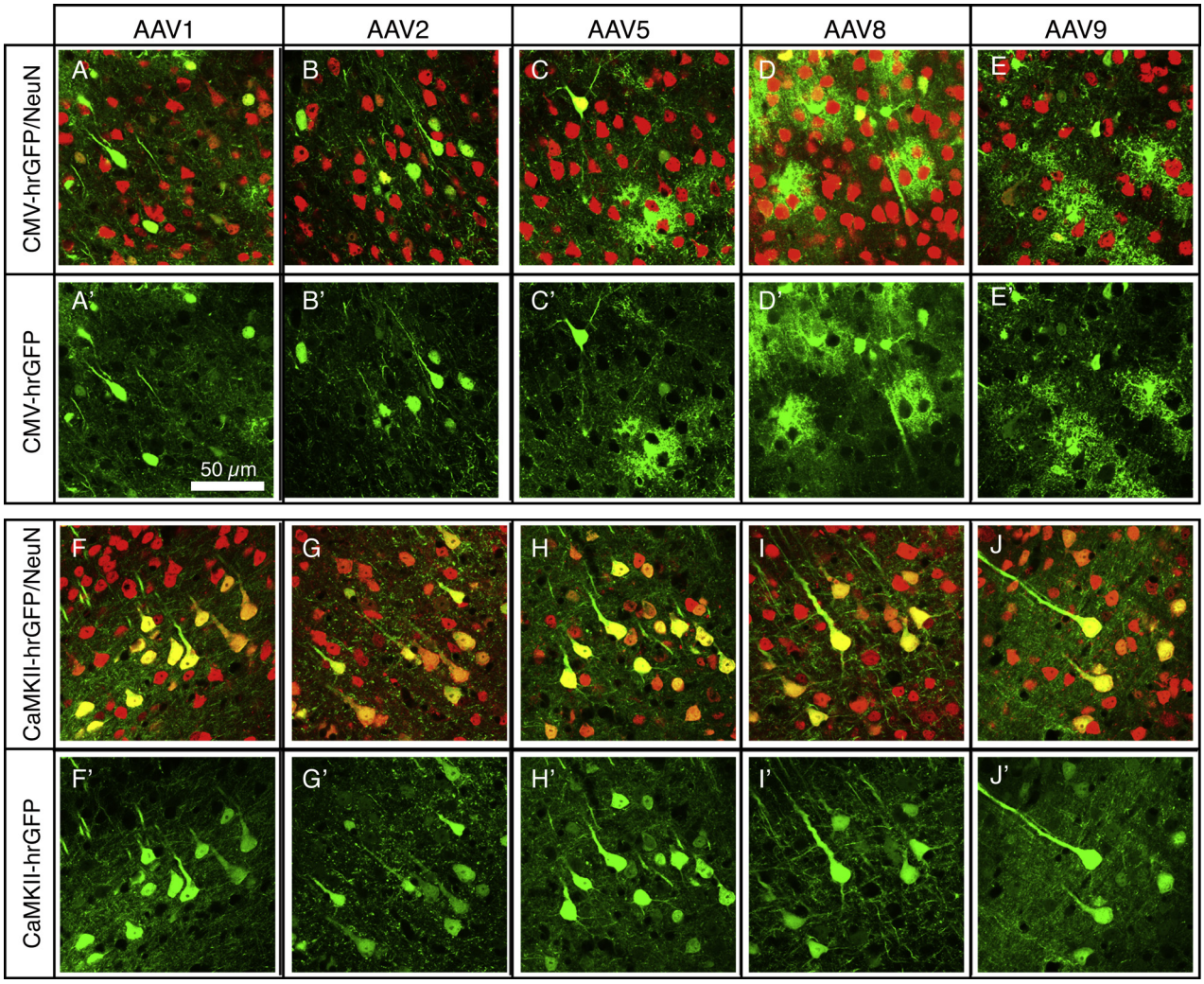

Fig. 8. Glial and neuronal expression of transgene from AAV serotypes in mouse cortex. Mouse cortical sections were immunostained with anti-hrGFP (green) and anti-NeuN antibody (red) to differentiate neuronal and glial transduction. A single optical section of confocal microscopy images are shown in each panel. These images were taken from layer 5. (For interpretation of the references to color in this figure legend, the reader is referred to the web version of this article.)

three-week waiting period (Table 1). At this time point, we already observed heavy accumulation of glia-like cells in the transduced regions for AAV8 (data not shown). Such glial accumulations were not observed for AAV1. However, when we extended the waiting period for six weeks for AAV1 and 9, we observed almost complete loss of NeuN signals and infiltration of glias into the infected area (Fig. 4C and D).

There is a possibility that the toxic effect is due to AAV infection itself rather than high hrGFP expression. To address this question, we examined the NeuN expression for CaMKII-hrGFP and SynI-hrGFP constructs, which had six week waiting period after infection. As shown in Fig. 4E–H, we did not observe adverse effects on NeuN expression for these constructs even after six weeks. We also did not observe accumulation of glia cells for AAV1-CaMKII, AAV1-SynI or AAV9-SynI constructs, although we observed glial accumulation in the vicinity of potential needle scar for AAV9-CaMKII construct (Fig. 4E–H). At higher magnification, we observed that NeuN expression is not necessarily downregulated in hrGFP-positive neurons for CamKII or SynI constructs (Fig. 4I and J). We conclude that AAV infection at the current titer (2.5×10^9 GC/0.5 μl) does not itself have toxic effects on neurons, although high-level transgene expression from the CMV construct may be toxic to neurons.

3.5. Cell type preference of CaMKII and SynI promoters

In a previous study, CaMKII and SynI constructs in AAV1 serotype exhibited preferential expression in excitatory and inhibitory neurons, respectively, in the mouse cortex at low dosage (Nathanson et al., 2009). In Fig. 5, we compared the properties of CaMKII and SynI promoters in side-by-side comparison. Fig. 5A shows a fluorescent image of the brain of marmoset #4, which received injections of CaMKII and SynI constructs on left and right hemispheres, respectively. As this overview image shows, the intensity of SynI promoter construct appeared to be lower than CaMKII constructs. At higher magnification, however, the fluorescent intensity of these two constructs did not appear different so much (Fig. 5B–E). One difference of the two promoters was that CaMKII construct exhibited relatively uniform expression throughout layers (Fig. 5B for AAV1, Fig. 5D for AAV9), as opposed to layer 3 and 5-enriched expression of SynI construct (Fig. 5C for AAV1, Fig. 5E for AAV9). The hrGFP expression from SynI construct was prevalent in only a limited population outside layers 3 and 5 (Fig. 5F–I).

To confirm the cell-type specific expression from these constructs, we tested the colocalization of hrGFP from CaMKII and SynI constructs with parvalbumin (PV), which is the major GABAergic

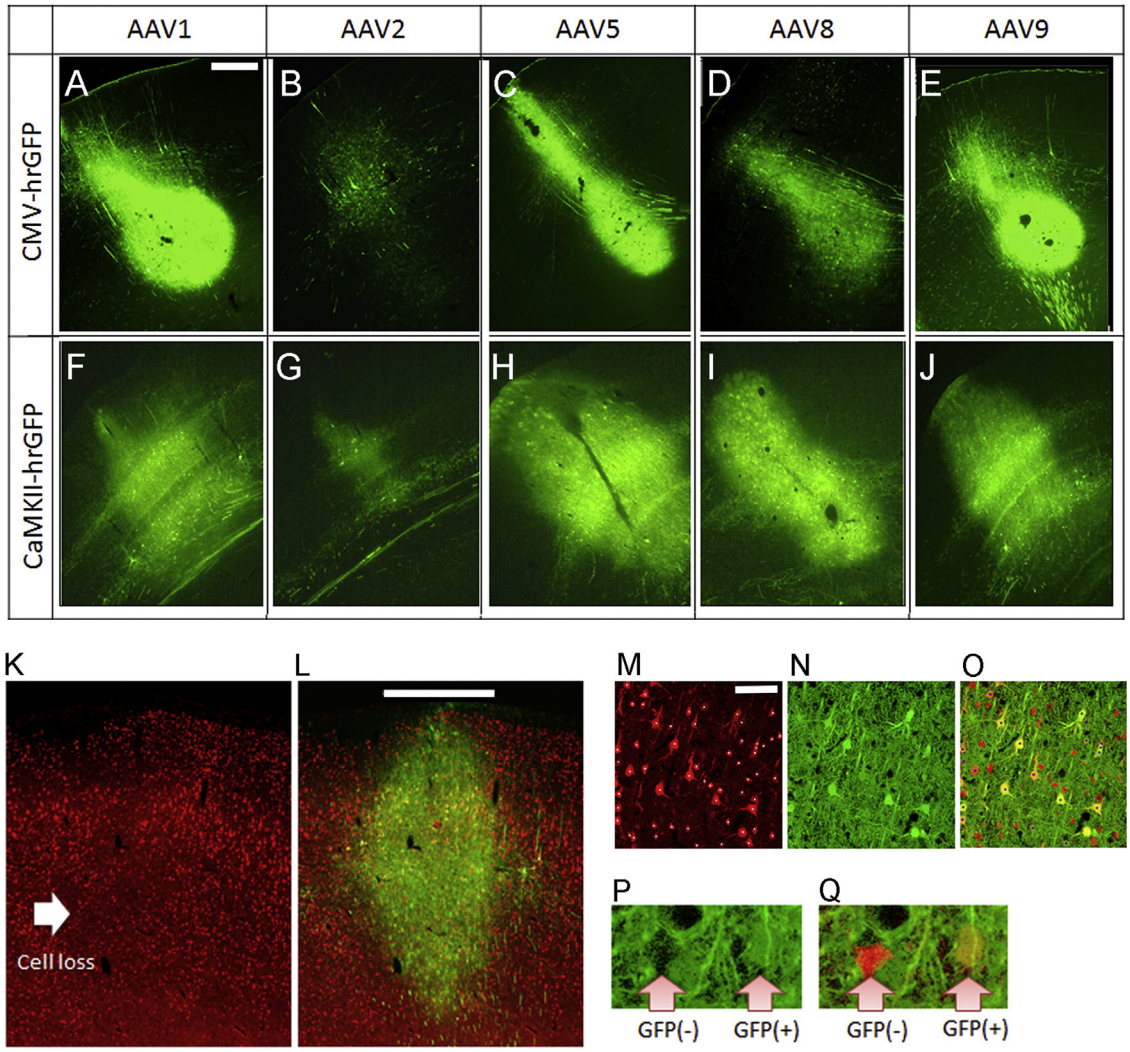

Fig. 9. AAV serotypes injected into the macaque cortex. (A–J) AAV constructs containing CMV and CaMKII promoters driving hrGFP expression were packaged in AAV1, 2, 5, 8, and 9 capsids and injected into the macaque cortex (V1). Each vector solution was injected at one site in each track. The low-magnified images of representative sections are shown for each combination. To aid visualization, the contrasts of images are adjusted to enable direct comparison of the signal intensities across serotypes. The sections for the same promoters were simultaneously imaged and contrast-adjusted in exactly the same conditions. (K and L) The NeuN and hrGFP-NeuN merged views of the M1 at 8 weeks following injection of AAV1 with CMV promoter, respectively. Note low expression of NeuN around the center of the injection site, which suggests cell loss. (M–Q) Higher magnification view of NeuN (M), hrGFP (N) and merged (O) views of layer 5 in macaque M1 following injection of AAV1 constructs containing CMV promoter. Further enlarged view emphasizing two neurons (one with and the other without the GFP expression) in P (hrGFP) and Q (merged), respectively. Scale bar in A, L and M shows 500 μm, 2 mm and 200 μm, respectively.

inhibitory neuron subtype marker. For the CaMKII construct, it was obvious that many PV-negative neurons express hrGFP (Fig. 6B–D). At the same time, the PV-positive neurons also expressed hrGFP at high efficiency (Fig. 6E–G: arrowheads). For SynI construct, the strongly positive cells outside layers 3 and 5 coincided surprisingly well with the PV-positive neurons (Fig. 6I–Q: arrowheads), supporting the previous findings in the mouse cortex. On the other hand, large pyramidal cells in layers 3 and 5 exhibited very high level of hrGFP (Fig. 6O–Q: arrows).

3.6. Transduction of mouse cortical cells by AAV serotypes

To compare the properties of AAV transduction between marmoset and mouse, we injected the same AAV preparations to the barrel cortex of mouse brains and counterstained with NeuN antibody. Figs. 7 and 8 shows the low and high-power views of the same set of AAV injection, as that shown for marmoset in Figs. 1 and 3. The overall feature of AAV transduction was similar between mouse and marmoset. First, AAV2 transduction area was smaller compared with other serotypes (Fig. 7). Second, as in marmoset, the widespread transduction in layers 2 and 5 occurred in some injections for AAV1, 8 and 9. At higher magnification, we could observe the transduction efficiency at the cellular level. Similar to the marmoset case, transduction by CMV-hrGFP construct resulted in very few NeuN-positive cells to exhibit hrGFP expression. One notable difference between mouse and marmoset was the morphology of glia cells transduced by AAV. Whereas the marmoset glia cells transduced by CMV-hrGFP exhibited conspicuous cell bodies and processes that almost look like neurons and were often attached to neuronal cells, the transduced mouse glia cells exhibited highly branched morphology (Fig. 8C′–E′). These may correspond to oligodendrocyte and astroglia, respectively. CaMKII construct in mouse cortex transduced neurons efficiently and looked quite similar to the patterns in marmoset cortex.

3.7. Transduction of macaque cortical cells by AAV serotypes

To compare the properties of AAV transduction between marmoset and macaque monkeys, we injected the same AAV preparations to either the primary visual cortex (V1) or motor cortex (M1)

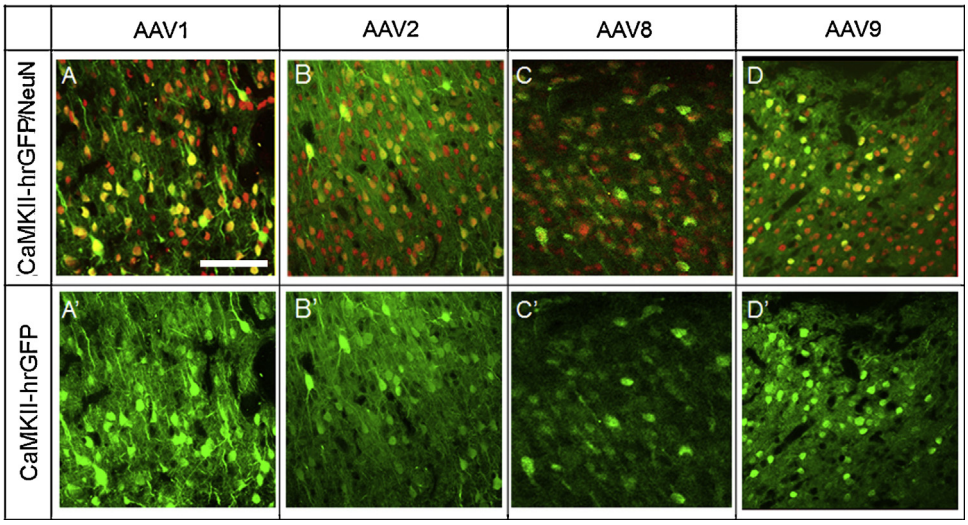

Fig. 10. Neuronal expression of transgene from AAV serotypes in macaque cortex. Macaque cortical sections were immunostained with anti-hrGFP (green) and anti-NeuN (red) antibodies to identify neuronal transduction. A single optical section of confocal microscopy images are shown in each panel. These images were taken from V1. Scale bar in A shows 20 μm. (For interpretation of the references to color in this figure legend, the reader is referred to the web version of this article.)

of macaque brains. Fig. 9A–J shows the low-power view of the cortical tissue around the injection sites of each serotype either with CMV (Fig. 9A–E) or with CaMKII (Fig. 9F–J) promoter. The overall feature of AAV transduction was similar between the macaque and marmoset. AAV2 transduction area was weaker compared with other serotypes (Fig. 9B and G). However, the widespread transduction in layers 2 and 5 was not as obvious as that in the mouse or marmoset. At higher magnification, we could observe the transduction efficiency at the cellular level. Similar to the marmoset, transduction by CMV-hrGFP construct was low (Fig. 9M–Q) in NeuN-positive cells to exhibit hrGFP expression and tissue damage was commonly found 8 weeks after the injection (Fig. 9K and L). In contrast, CaMKII construct in the macaque cortex did not much cause damage and its transduction efficiency was higher than the CMV construct. The efficiency of hrGFP transduction in NeuN-positive cells was similar to that of the marmosets (Fig. 10; AAV1; 73.4%, AAV2; 67.6%, AAV8; 41.3%, AAV9; 70.3%).

4. Discussion

Choosing the right serotype for transduction is a key step for successful manipulation of cortical cells. For this purpose, we performed a series of injections for AAV1, 2, 5, 8 and 9 serotypes in marmoset, mouse and macaque cortex. There are many precedents of reports that investigated the transduction properties of various AAV serotypes in the cerebral cortex (Cearley and Wolfe, 2006; Nathanson et al., 2009; Masamizu et al., 2010, 2011; Hutson et al., 2012; Aschauer et al., 2013; Wang et al., 2014). What is new in the current study is that we used neuron-specific CaMKII promoter for systematic comparison of serotypes. Most of past studies, except a few (Nathanson et al., 2009; Holehonnur et al., 2014), used ubiquitous promoters, such as CMV and CAG promoters, for serotype evaluation. We found that the use of CaMKII promoter is advantageous in two respects. First, we were able to examine the efficiency of neuronal transduction without the interference of glial expression. Second, we observed potential toxicity and inflammation caused by the high-level transgene expression for CMV-construct but not for CaMKII construct. By avoiding the problem of glial expression and toxicity, we reached the conclusion that AAV1, 2, 5, 8 and 9 can all efficiently transduce neurons in marmoset, mouse and macaque cerebral cortex. Among these serotypes, AAV2 tended to spread smaller than other serotypes, and AAV5 expressed lower level of transgene than other serotypes (see Fig. 1). Other than that, the behavior of AAV1, 8 and 9 did not differ significantly, at least for the CaMKII construct.

One important observation that emerged from the current study is that the expression levels of the transduced neurons are variable and that many neurons with low transgene expression are buried in the matrices of transgene-positive neuropils that fill the space between the cell bodies. This observation was made possible by the use of CaMKII promoter and may have been overlooked in past studies. What is the cause for variable expression level among neurons? One possibility is the different activity of promoters in different cell types. Nathanson et al. reported that SynI and CaMKII promoters in AAV1 serotype exhibit higher transcription activity in inhibitory and excitatory neurons, respectively, at low dosage (Nathanson et al., 2009). Indeed, we found a tendency for higher expression in parvalbumin-positive inhibitory neurons from SynI promoter (Fig. 6). But we also observed strong expression from the SynI construct in large pyramidal cells of layers 3 and 5 (Fig. 5E). Compared with SynI promoter, the CaMKII promoter exhibited more diffuse pattern, which suggest uniform transduction of excitatory neurons. But CaMKII construct also transduced inhibitory neurons (Fig. 6). To conclude, CaMKII and SynI promoters exhibit somewhat different cell type-specific activity. But they are active both in excitatory and inhibitory neurons, and cannot explain the variability among the transduced neurons.

Another possibility for different expression level is the difference in multiplicity of transduction. We believe that over ~70% of the neurons are transduced by AAV in our conditions. But the multiplicity of viral infection could be different among neurons and it may lead to differential transgene expression. In the marmoset cortex, we observed generally high-level transgene expression in large pyramidal cells in layers 3 and 5 (e.g., see Fig. 4). This tendency was most conspicuous for SynI promoter but was observed regardless of promoters, including CMV promoter. We speculate that large pyramidal cells may allow more viral entries via their widespread dendritic fields. In support of this idea, the sparse but widespread transduction occurred in large pyramidal cells of layer 5 well beyond the core region (Fig. 2J). Interestingly, Nathanson et al. reported that excitatory/inhibitory preference of SynI construct dramatically changes by the titer of the viral solution (Nathanson et al., 2009). In addition, they also observed preferential expression in layer 5 pyramidal cells (in addition to GABAergic cells) in the mouse cortex from SynI promoter when the viral titer is low. This observation is consistent with our idea

that multiplicity of infection affects the apparent cell type preference.

We have shown here that viral spread is smaller for AAV2 than other serotypes, which is supported by many reports in various systems (Klein et al., 2006; Aschauer et al., 2013; Burger et al., 2004; Hutson et al., 2012; McFarland et al., 2009; Taymans et al., 2007; McFarland et al., 2009; Hutson et al., 2012). However, we do not completely understand why the injection of the same viral preparations led to variable results as we have shown in Fig. 2. For one thing, technical difficulty of accurate injection (e.g., leak from the hole, or clogging of the glass needle) may have led to variability. Another possible reason is that the different cellular and fiber architecture of the injected tissues may have affected the dispersion of the viral particles. In a previous study, the relative efficiency of AAV infection was different between striatum, hippocampus and cortex of the mouse brain, which have very different cytoarchitectures (Aschauer et al., 2013). It is possible that the areas with different laminar depths and fibrous architecture may exhibit difference in AAV spread. We have also yet to clarify the parameters that led to unusually widespread transduction in the upper layer in some injections, which could be useful for many experimental applications.

It is previously reported that high-level expression of GFP in substantia nigra neurons by AAV8 lead to cell death (Klein et al., 2006). Our data also support the toxicity of high-level transgene expression (Fig. 4). We suspect that one possible reason for very different cell tropism of AAV8 reported in this and previous study (Masamizu et al., 2010, 2011) may stem from difference in the extent of cell death and infiltration of glial cells. In our experiment for CMV construct, we observed presence of glia-like cells in transduced areas for AAV 5 and 8, even at three weeks of injection (data not shown). We cannot deny the possibility that there exist some impurity that can only be removed by column chromatographic purification and lead to inflammation (Klein et al., 2008). Alternatively, the chromatographic purification may distinguish two populations of AAV particles that have differential affinity to neurons and glias. Another factor to be considered is the toxicity of the transgene itself. Wallace et al. reported that high-level expression of hrGFP is more toxic than eGFP to muscle cells (Wallace et al., 2013). Thus, potential toxicity of transgene needs to be considered carefully to choose serotype and promoters for experiment. In this context, the relatively low level expression of transgene from AAV5 may have been advantageous for long-term experiments encountered in primates (Diester et al., 2011).

Finally, we comment on the comparison of species in serotype properties. To our knowledge, this is the first report that directly tested the transduction properties of the same viral preparations in different species. In all the species, transduction of AAV2 was low, while that of AAV1, 5, 8 and 9 was similarly high. As far as the CaMKII construct is concerned, we did not observe very big differences among mice, marmosets and macaque monkeys. As for the CMV promoter, AAV1 was more neuronal than glial in mice, whereas it was predominantly glial in marmoset. In the macaque, the AAV transduction was observed in both neuronal and glial cells. AAV5, 8 and 9 was glial in both mouse and marmoset, but the morphology suggests that the former is astroglia, while the latter is oligodendrocyte. Such species differences may occur as combined effects of differences in cortical architecture (e.g., width of layers, density of cellular components and/or axonal fibers, etc.), ratio of cell types (neuronal and glial subtypes), and promoter activity in each cell type.

Acknowledgements

We thank Drs. Ryosuke Matsui and Dai Watanabe, Kyoto University for CaMKII promoter DNA. We thank Ms. Ohsawa for help with histology and confocal microscope imaging. Confocal images were acquired at Spectrography and Bioimaging Facility, NIBB Core Research Facilities. Some of the monkeys used in this study were provided by the National BioResource Project 'Japanese Monkeys' of the Ministry of Education, Culture, Sports, Science and Technology, Japan. This study is the result of "Highly creative animal model development for brain sciences" carried out under the Strategic Research Program for Brain Sciences by the Ministry of Education, Culture, Sports, Science and Technology of Japan. Also supported by Scientific Research on Innovative Areas (Neocortical Organization) (22123009 to TY and 23123510 to HH) and the grant from the JSPS (Japan Society for the Promotion of Science) to AW (KAKENHI 40290910 and 22500300), and Grants-in-Aid for Scientific Research A (20240030) to TY.

References

Aschauer, D.F., Kreuz, S., Rumpel, S., 2013. Analysis of transduction efficiency, tropism and axonal transport of AAV serotypes 1, 2, 5, 6, 8 and 9 in the mouse brain. PLOS ONE 8, e76310.

Bendor, D., Wang, X., 2005. The neuronal representation of pitch in primate auditory cortex. Nature 436, 1161–1165.

Betley, J.N., Sternson, S.M., 2011. Adeno-associated viral vectors for mapping, monitoring, and manipulating neural circuits. Hum. Gene Ther. 22, 669–677.

Blits, B., Derks, S., Twisk, J., Ehlert, E., Prins, J., Verhaagen, J., 2010. Adeno-associated viral vector (AAV)-mediated gene transfer in the red nucleus of the adult rat brain: comparative analysis of the transduction properties of seven AAV serotypes and lentiviral vectors. J. Neurosci. Methods 185, 257–263.

Burger, C., Gorbatyuk, O.S., Velardo, M.J., Peden, C.S., Williams, P., Zolotukhin, S., Reier, P.J., Mandel, R.J., Muzyczka, N., 2004. Recombinant AAV viral vectors pseudotyped with viral capsids from serotypes 1, 2, and 5 display differential efficiency and cell tropism after delivery to different regions of the central nervous system. Mol. Ther. 10, 302–317.

Cearley, C.N., Wolfe, J.H., 2006. Transduction characteristics of adeno-associated virus vectors expressing cap serotypes 7, 8, 9, and Rh10 in the mouse brain. Mol. Ther. 13, 528–537.

Clarke, H.F., Dalley, J.W., Crofts, H.S., Robbins, T.W., Roberts, A.C., 2004. Cognitive inflexibility after prefrontal serotonin depletion. Science 304, 878–880.

Diester, I., Kaufman, M.T., Mogri, M., Pashaie, R., Goo, W., Yizhar, O., Ramakrishnan, C., Deisseroth, K., Shenoy, K.V., 2011. An optogenetic toolbox designed for primates. Nat. Neurosci. 14, 387–397.

Dodiya, H.B., Bjorklund, T., Stansell, J.r., Mandel, R.J., Kirik, D., Kordower, J.H., 2010. Differential transduction following basal ganglia administration of distinct pseudotyped AAV capsid serotypes in nonhuman primates. Mol. Ther. 18, 579–587.

Fenno, L., Yizhar, O., Deisseroth, K., 2011. The development and application of optogenetics. Annu. Rev. Neurosci. 34, 389–412.

Han, X., 2012. Optogenetics in the nonhuman primate. Prog. Brain Res. 196, 215–233.

Hioki, H., Kuramoto, E., Konno, M., Kameda, H., Takahashi, Y., Nakano, T., Nakamura, K.C., Kaneko, T., 2009. High-level transgene expression in neurons by lentivirus with Tet-Off system. Neurosci. Res. 63, 149–154.

Holehonnur, R., Luong, J.A., Chaturvedi, D., Ho, A., Lella, S.K., Hosek, M.P., Ploski, J.E., 2014. Adeno-associated viral serotypes produce differing titers and differentially transduce neurons within the rat basal and lateral amygdala. BMC Neurosci. 15, 28.

Hutson, T.H., Verhaagen, J., Yanez-Munoz, R.J., Moon, L.D., 2012. Corticospinal tract transduction: a comparison of seven adeno-associated viral vector serotypes and a non-integrating lentiviral vector. Gene Ther. 19, 49–60.

Kinoshita, M., Matsui, R., Kato, S., Hasegawa, T., Kasahara, H., Isa, K., Watakabe, A., Yamamori, T., Nishimura, Y., Alstermark, B., Watanabe, D., Kobayashi, K., Isa, T., 2012. Genetic dissection of the circuit for hand dexterity in primates. Nature 487, 235–238.

Klein, R.L., Dayton, R.D., Leidenheimer, N.J., Jansen, K., Golde, T.E., Zweig, R.M., 2006. Efficient neuronal gene transfer with AAV8 leads to neurotoxic levels of tau or green fluorescent proteins. Mol. Ther. 13, 517–527.

Klein, R.L., Dayton, R.D., Tatom, J.B., Henderson, K.M., Henning, P.P., 2008. AAV8, 9, Rh10, Rh43 vector gene transfer in the rat brain: effects of serotype, promoter and purification method. Mol. Ther. 16, 89–96.

Lock, M., McGorray, S., Auricchio, A., Ayuso, E., Beecham, E.J., Blouin-Tavel, V., Bosch, F., Bose, M., Byrne, B.J., Caton, T., Chiorini, J.A., Chtarto, A., Clark, K.R., Conlon, T., Darmon, C., Doria, M., Douar, A., Flotte, T.R., Francis, J.D., Francois, A., Giacca, M., Korn, M.T., Korytov, I., Leon, X., Leuchs, B., Lux, G., Melas, C., Mizukami, H., Moullier, P., Muller, M., Ozawa, K., Philipsberg, T., Poulard, K., Raupp, C., Riviere, C., Roosendaal, S.D., Samulski, R.J., Soltys, S.M., Surosky, R., Tenenbaum, L., Thomas, D.L., van Montfort, B., Veres, G., Wright, J.F., Xu, Y., Zelenaia, O., Zentilin, L., Snyder, R.O., 2010. Characterization of a recombinant adeno-associated virus type 2 Reference Standard Material. Hum. Gene Ther. 21, 1273–1285.

Markakis, E.A., Vives, K.P., Bober, J., Leichtle, S., Leranth, C., Beecham, J., Elsworth, J.D., Roth, R.H., Samulski, R.J., Redmond, D.E.J., 2010. Comparative transduction efficiency of AAV vector serotypes 1–6 in the substantia nigra and striatum of the primate brain. Mol. Ther. 18, 588–593.

Masamizu, Y., Okada, T., Ishibashi, H., Takeda, S., Yuasa, S., Nakahara, K., 2010. Efficient gene transfer into neurons in monkey brain by adeno-associated virus 8. Neuroreport 21, 447–451.

Masamizu, Y., Okada, T., Kawasaki, K., Ishibashi, H., Yuasa, S., Takeda, S., Hasegawa, I., Nakahara, K., 2011. Local and retrograde gene transfer into primate neuronal pathways via adeno-associated virus serotype 8 and 9. Neuroscience 193, 249–258.

McFarland, N.R., Lee, J.S., Hyman, B.T., McLean, P.J., 2009. Comparison of transduction efficiency of recombinant AAV serotypes 1, 2, 5, and 8 in the rat nigrostriatal system. J. Neurochem. 109, 838–845.

Nathanson, J.L., Yanagawa, Y., Obata, K., Callaway, E.M., 2009. Preferential labeling of inhibitory and excitatory cortical neurons by endogenous tropism of adeno-associated virus and lentivirus vectors. Neuroscience 161, 441–450.

Okano, H., Hikishima, K., Iriki, A., Sasaki, E., 2012. The common marmoset as a novel animal model system for biomedical and neuroscience research applications. Semin. Fetal Neonatal Med. 17, 336–340.

Rabinowitz, J.E., Rolling, F., Li, C., Conrath, H., Xiao, W., Xiao, X., Samulski, R.J., 2002. Cross-packaging of a single adeno-associated virus (AAV) type 2 vector genome into multiple AAV serotypes enables transduction with broad specificity. J. Virol. 76, 791–801.

Sanchez, C.E., Tierney, T.S., Gale, J.T., Alavian, K.N., Sahin, A., Lee, J.S., Mulligan, R.C., Carter, B.S., 2011. Recombinant adeno-associated virus type 2 pseudotypes: comparing safety, specificity, and transduction efficiency in the primate striatum. Laboratory investigation. J. Neurosurg. 114, 672–680.

Taymans, J.M., Vandenberghe, L.H., Haute, C.V., Thiry, I., Deroose, C.M., Mortelmans, L., Wilson, J.M., Debyser, Z., Baekelandt, V., 2007. Comparative analysis of adeno-associated viral vector serotypes 1, 2, 5, 7, and 8 in mouse brain. Hum. Gene Ther. 18, 195–206.

Wang, Q., Henry, A.M., Harris, J.A., Oh, S.W., Joines, K.M., Nyhus, J., Hirokawa, K.E., Dee, N., Mortrud, M., Parry, S., Ouellette, B., Caldejon, S., Bernard, A., Jones, A.R., Zeng, H., Hohmann, J.G., 2014. Systematic comparison of adeno-associated virus and biotinylated dextran amine reveals equivalent sensitivity between tracers and novel projection targets in the mouse brain. J. Comp. Neurol. 522, 1989–2012.

Wallace, L.M., Moreo, A., Clark, K.R., Harper, S.Q., 2013. Dose-dependent toxicity of humanized *Renilla reniformis* GFP (hrGFP) limits its utility as a reporter gene in mouse muscle. Mol. Ther. Nucleic Acids 2, e86.

Watakabe, A., Kato, S., Kobayashi, K., Takaji, M., Nakagami, Y., Sadakane, O., Ohtsuka, M., Hioki, H., Kaneko, T., Okuno, H., Kawashima, T., Bito, H., Kitamura, Y., Yamamori, T., 2012. Visualization of cortical projection neurons with retrograde TET-off lentiviral vector. PLOS ONE 7, e46157.

Wu, Z., Asokan, A., Samulski, R.J., 2006. Adeno-associated virus serotypes: vector toolkit for human gene therapy. Mol. Ther. 14, 316–327.

Yagi, H., Ogura, T., Mizukami, H., Urabe, M., Hamada, H., Yoshikawa, H., Ozawa, K., Kume, A., 2011. Complete restoration of phenylalanine oxidation in phenylketonuria mouse by a self-complementary adeno-associated virus vector. J. Gene Med. 13, 114–122.

Yamamori, T., Rockland, K.S., 2006. Neocortical areas, layers, connections, and gene expression. Neurosci. Res. 55, 11–27.